

# Ferrimagnetic charge order in molecular conductors with diluted localized spins exhibiting enhanced giant magnetoresistance effect

Ryuta Ishii,<sup>1</sup> Misato Uejo,<sup>2</sup> Erina Watari,<sup>2</sup> Mitsuo Ikeda,<sup>1</sup> Hiroshi Murakawa,<sup>1</sup> Hideaki Sakai<sup>ⓧ</sup>,<sup>1</sup> Masaki Matsuda,<sup>3</sup> Hideo Yoshioka,<sup>2,\*</sup> Masahisa Tsuchiizu,<sup>2,†</sup> and Noriaki Hanasaki<sup>ⓧ</sup><sup>1,4,‡</sup>

<sup>1</sup>Department of Physics, Osaka University, Toyonaka, Osaka 560-0043, Japan

<sup>2</sup>Department of Physics, Nara Women's University, Nara 630-8506, Japan

<sup>3</sup>Department of Chemistry, Graduate School of Science and Technology, Kumamoto University, Kumamoto 860-8506, Japan

<sup>4</sup>Spintronics Research Network Division, Institute for Open and Transdisciplinary Research Initiatives, Osaka University, Suita, Osaka 565-0871, Japan



(Received 6 September 2023; accepted 23 October 2023; published 9 November 2023)

In phthalocyanine molecular conductors, the giant magnetoresistance effect is enhanced by the dilution of the localized-spin density. At low spin density, the localized spin induces a random potential for the conduction electron. The charge gap increases as spin density reaches intermediate levels. Analyses based on the mean-field theory and the exact-diagonalization method reveal that the ferrimagnetic charge-ordered state grows above the threshold localized-spin density. The localized spins assist in the ferromagnetic superexchange interaction, consistent with the measured spontaneous magnetization. Various electronic states compete with each other, and the coherent part of the optical conductivity is enhanced by the weak magnetic field. These theoretical findings are in stark agreement with the observed giant magnetoresistance.

DOI: [10.1103/PhysRevB.108.205114](https://doi.org/10.1103/PhysRevB.108.205114)

## I. INTRODUCTION

The gigantic response to external stimuli is an interesting phenomenon in condensed matter physics. The giant magnetoresistance effect is observed in both the magnetic superlattice and manganese oxides [1,2]. In the case of the latter materials, when the  $e_g$  electron band is half filled, the on-site Coulomb interaction leads to a Mott insulating state. In the case of the quarter filling in the  $e_g$  orbitals, the nearest-neighbor Coulomb interaction drives the charge order. The  $t_{2g}$  localized spin having an antiferromagnetic correlation leads to the reduction of the transfer energy of the  $e_g$  conduction electron. In the magnetic field, the  $t_{2g}$  localized spins are aligned, and the transfer energy is enhanced through Hund's coupling. This results in the transition from the Mott/charge-order insulating state to the ferromagnetic metallic state, giving rise to the giant/colossal magnetoresistance effect [3]. The correlation between the neighboring localized spins is an important factor for the gigantic response in magnetotransport phenomena. If the localized spins are diluted, the network of antiferromagnetic interactions between them is partially disrupted. This could potentially lead to a reduction in the magnetic-field strength required to align the localized spins and an increased likelihood of enhancing the magnetoresistance effect. However, the impact of localized spin dilution on the electronic state and the magnetoresistance effect remains uncertain. Due to the challenge of maintaining the filling of

$e_g$  conduction electrons while diluting  $t_{2g}$  localized spins in transition metal oxides, the correlation with localized-spin density has yet to be explored.

The flexible molecular design provides an opportunity for the detailed study of the localized-spin effect [4–9]. The ligated metal phthalocyanine molecule  $M(\text{Pc})(\text{CN})_2$  accommodates the conduction electron and the localized spins [10]. The molecular structure of  $M(\text{Pc})(\text{CN})_2$  is displayed in Fig. 1(a). Here,  $M$  and Pc denote the transition metal ion and phthalocyanine, which is the ring part of the molecule, respectively. The Pc molecular ring provides  $\pi$  conduction electrons, and the transition metal ion  $M$  can possess  $d$  localized spins. It is possible to control the density of  $d$  localized spins by substituting the transition metal ion  $M$ . For  $M = \text{Fe}$  and  $\text{Cr}$ , a  $d$  localized spin exists with values of  $S = 1/2$  (Ising spin) and  $3/2$  (Heisenberg spin), respectively. Conversely,  $M = \text{Co}$  displays nonmagnetic behavior [10,11]. The intramolecular interaction  $J_{\pi d}$  between the  $\pi$  conduction electron and the  $d$  localized spin in  $M = \text{Fe}$  and  $\text{Cr}$  is ferromagnetic in nature. This interaction is akin to the Hund's coupling observed in manganese oxides [12,13].

In molecular conductor  $\text{TPP}[M(\text{Pc})(\text{CN})_2]_2$ , the  $M(\text{Pc})(\text{CN})_2$  molecules stack along the  $c$  axis, as displayed in Fig. 1(b). The highest occupied molecular orbital of the  $\pi$  conduction electron is spread in the ring part of the Pc molecule. As seen in the figure, there is an overlap of the  $\pi$  orbitals of these ring parts between the neighboring molecules, leading to the one-dimensional conduction. Here, TPP denotes tetraphenylphosphonium, which is a closed-shell molecule. The intermolecular Coulomb interaction  $V$  drives the charge order of the  $\pi$  conduction electron, as illustrated in Fig. 1(c) [14–18]. In the figure, the sizes of the circles

\*Corresponding author: [h-yoshi@cc.nara-wu.ac.jp](mailto:h-yoshi@cc.nara-wu.ac.jp)

†Corresponding author: [tsuchiiz@cc.nara-wu.ac.jp](mailto:tsuchiiz@cc.nara-wu.ac.jp)

‡Corresponding author: [hanasaki@phys.sci.osaka-u.ac.jp](mailto:hanasaki@phys.sci.osaka-u.ac.jp)

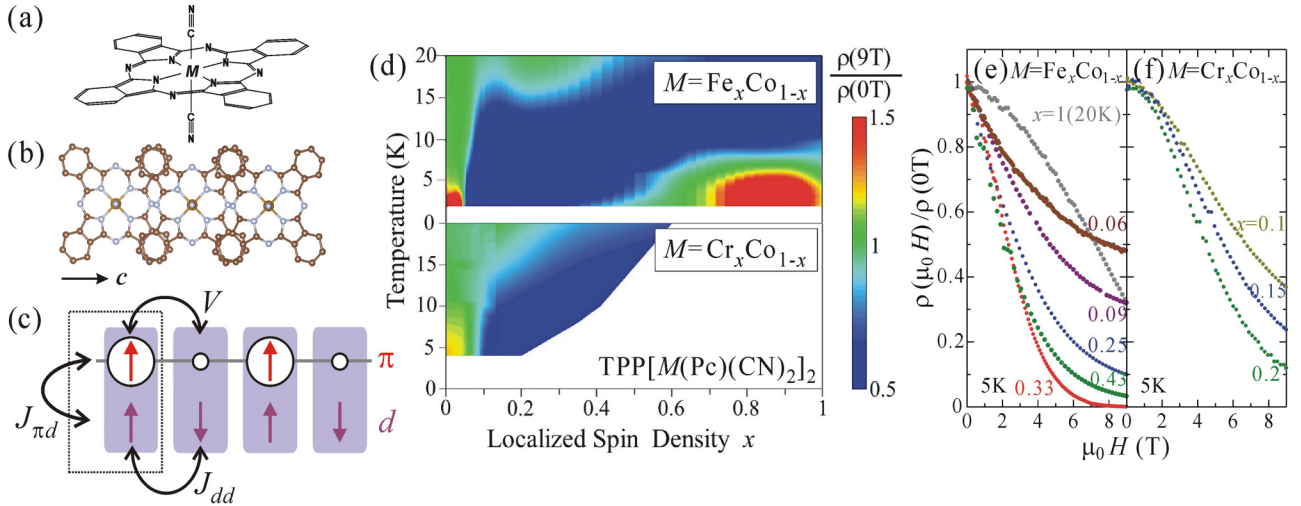


FIG. 1. (a) Molecular structure of the ligated metal phthalocyanine  $M(\text{Pc})(\text{CN})_2$ . (b) Molecular stacking of  $M(\text{Pc})(\text{CN})_2$  along the  $c$  axis. (c) Illustration of the  $\pi$  conduction electron,  $d$  localized spin, and their interactions. The red and purple arrows indicate the spin state of the  $\pi$  conduction electron and  $d$  localized spin, respectively. The sizes of the circles indicate the amount of charge in the  $\pi$  conduction electron.  $V$ ,  $J_{\pi d}$ , and  $J_{dd}$  denote the Coulomb interaction in the  $\pi$  conduction electrons between the neighboring molecules, the intramolecular ferromagnetic interaction between the  $\pi$  conduction electron and  $d$  localized spin, and the intermolecular antiferromagnetic interaction between the  $d$  localized spins, respectively. (d) Color contour plot of the magnetoresistance in  $M = \text{Fe}_x\text{Co}_{1-x}$  (upper panel) and  $M = \text{Cr}_x\text{Co}_{1-x}$  (lower panel) of  $\text{TPP}[M(\text{Pc})(\text{CN})_2]_2$ . The red (blue) color indicates positive (negative) magnetoresistance. (e), (f) Magnetoresistance as a function of the magnetic field at 5 K in  $M = \text{Fe}_x\text{Co}_{1-x}$  and  $M = \text{Cr}_x\text{Co}_{1-x}$ , respectively.

in the  $\pi$  conduction electron indicate the amount of charge. Even when the charge order in the  $\pi$  conduction electron is made, the formation of the electric dipole moment and the ferroelectricity are not anticipated, since the intermolecular distance is the same in every molecule along the  $c$  axis. In  $M = \text{Fe}$ , the antiferromagnetic order of the  $d$  localized spins existing in every site stabilizes the charge order of the  $\pi$  conduction electron through the intramolecular ferromagnetic interaction  $J_{\pi d}$  [19,20]. When this antiferromagnetic state is suppressed by applying the magnetic field, the stability of the charge order is reduced, leading to the giant magnetoresistance effect [21,22].

Through the partial substitution of  $\text{Co}(\text{Pc})(\text{CN})_2$ , a compound lacking localized spins, in place of  $\text{Fe}(\text{Pc})(\text{CN})_2$ , it becomes possible to investigate the correlation with localized-spin density [23]. Figure 1(d) displays the color contour plot of the magnetoresistance effect in  $M = \text{Fe}_x\text{Co}_{1-x}$  and  $\text{Cr}_x\text{Co}_{1-x}$  of  $\text{TPP}[M(\text{Pc})(\text{CN})_2]_2$ . Red and blue indicate positive and negative magnetoresistance, respectively. In the absence of localized spin ( $x = 0$ ), positive magnetoresistance is observed [24,25]. Significant negative magnetoresistance was observed not only in cases of high localized-spin density but also in instances of low localized-spin density. Figures 1(e) and 1(f) show the giant negative magnetoresistance in the low  $x$  range in  $M = \text{Fe}_x\text{Co}_{1-x}$  and  $M = \text{Cr}_x\text{Co}_{1-x}$ , respectively. At 5 K, the magnetoresistance ratio of  $\frac{\rho(9\text{T})}{\rho(0\text{T})}$  reaches 0.001 in  $M = \text{Fe}_{0.33}\text{Co}_{0.67}$  and 0.12 in  $M = \text{Cr}_{0.2}\text{Co}_{0.8}$ , respectively. The magnetoresistance effect is amplified by the dilution of the localized-spin density. In the low localized-spin density, the conventional magnetoresistance model is no longer relevant.

In this paper, we report the localized-spin-density dependence on the transport and magnetic properties in  $M = \text{Cr}_x\text{Co}_{1-x}$  and  $M = \text{Fe}_x\text{Co}_{1-x}$ , and investigate theoretically

their electronic states on the basis of the mean-field theory and the exact-diagonalization method. At localized-spin densities below  $x \approx 0.1$ , characterized as low, the  $d$  localized spins introduce a random magnetic potential for the  $\pi$  conduction electron. At intermediate densities above  $x \approx 0.1$ , the effective gap increases with the localized-spin density. In  $M = \text{Fe}_x\text{Co}_{1-x}$ , where Ising spin is present, spontaneous magnetization is observed, indicating the development of local order. The calculations in the mean-field theory show that the charge order is enhanced and that spontaneous magnetization is induced simultaneously by the  $d$  localized spins above the threshold density. To explain the origin of the spontaneous magnetization, we propose an interaction through the localized-spin site: *the localized-spin-assisted ferromagnetic superexchange interaction*. Based on the obtained experimental results and theoretical analyses, we discuss the mechanism underlying the giant magnetoresistance effect observed in the intermediate localized-spin density.

## II. EXPERIMENTAL METHODS

The molecular crystals  $M = \text{Cr}_x\text{Co}_{1-x}$  and  $M = \text{Fe}_x\text{Co}_{1-x}$  of  $\text{TPP}[M(\text{Pc})(\text{CN})_2]_2$  were synthesized by using the starting materials  $\text{TPP}[M(\text{Pc})(\text{CN})_2]$  ( $M = \text{Cr}, \text{Fe}, \text{and Co}$ ) and the solvent acetonitrile by the electrochemical method [23,26]. The crystal system was checked by using the Rigaku VariMax Rapid FR-E x-ray diffractometer. The magnetic susceptibility was measured by using the Quantum Design MPMS. Here, the formula unit is defined as  $\text{TPP}[\text{Cr}_x\text{Co}_{1-x}(\text{Pc})(\text{CN})_2]_2$  or  $\text{TPP}[\text{Fe}_x\text{Co}_{1-x}(\text{Pc})(\text{CN})_2]_2$ . Tens of crystals were measured, and these crystal axes were not aligned. By SEM-EDS, we made sure that the atomic ratio  $x$  of the mixed crystals  $M = \text{Cr}_x\text{Co}_{1-x}$  and  $M = \text{Fe}_x\text{Co}_{1-x}$  of  $\text{TPP}[M(\text{Pc})(\text{CN})_2]_2$  was close to the molar ratios of the starting materials. Both low

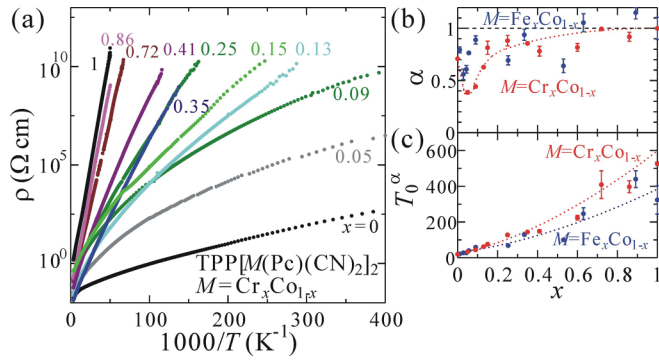


FIG. 2. (a) Temperature dependence of the resistivity in  $M = \text{Cr}_x\text{Co}_{1-x}$  of  $\text{TPP}[\text{M}(\text{Pc})(\text{CN})_2]_2$ . (b), (c) Dependence of  $\alpha$  and  $T_0^\alpha$  on the localized-spin density  $x$ , respectively. The red and blue circles indicate the data in  $M = \text{Cr}_x\text{Co}_{1-x}$  and  $M = \text{Fe}_x\text{Co}_{1-x}$ , respectively. The dashed curves are guides for the eye.

and high resistivities were determined using distinct methods: the four-probe method employing the Quantum Design PPMs for the former and the two-probe method utilizing the Keithley 6517 for the latter. The current was applied along the  $c$  axis.

### III. EXPERIMENTAL RESULTS

To reveal the electronic state in the low localized-spin density, we will analyze the electronic states on the basis of the transport and magnetic properties. Figure 2(a) shows the temperature dependence of the resistivity in  $M = \text{Cr}_x\text{Co}_{1-x}$ . At every localized-spin density  $x$ , the resistivity increases as the temperature decreases. The temperature dependence of the resistivity becomes clearly convex below  $x=0.3$ . A similar tendency is seen in  $M = \text{Fe}_x\text{Co}_{1-x}$  [23]. Since the  $\text{Cr}(\text{Pc})(\text{CN})_2/\text{Fe}(\text{Pc})(\text{CN})_2$  molecule with  $d$  localized spin and the  $\text{Co}(\text{Pc})(\text{CN})_2$  molecule without  $d$  localized spin exist randomly in the one-dimensional conduction path, the randomness of the magnetic potential for the  $\pi$  conduction electron is created. If one assumes the variable range hopping (VRH) model, the resistivity can be fitted by

$$\rho \sim \exp\left(\frac{T_0^\alpha}{T}\right). \quad (1)$$

Here, the  $T_0$  value corresponds to the activation energy in  $\alpha = 1$  and reflects the localization length in  $\alpha < 1$ . Figures 2(b) and 2(c) show  $\alpha$  and  $T_0^\alpha$  obtained by the fitting of the resistivity, respectively. The red and blue circles indicate the data of  $M = \text{Cr}_x\text{Co}_{1-x}$  and  $\text{Fe}_x\text{Co}_{1-x}$ , respectively. The decrement of the  $\alpha$  value from 1 reflects the randomness in the system. In  $x=1$ , the  $\alpha$  value is 1, since the  $d$  localized spins exist in every site. As the localized-spin density decreases below  $x=0.5$ , the  $\alpha$  value decreases, suggesting that the randomness increases. Near  $x \approx 0.1$ , the  $\alpha$  value reaches its lowest point, with values in the range of  $0.4 \sim 0.55$ . Note that  $\alpha = 0.5$  corresponds to the value theoretically given by the one-dimensional case ( $\alpha = \frac{1}{d+1}$  in  $d = 1$ ) of the VRH model. Here, the  $d$  value denotes the dimension of the electron conduction. In  $x \gtrsim 0.2$ , the  $T_0^\alpha$  value is enhanced with  $x$ , suggesting that the charge gap is enhanced when the spin density  $x$  increases.

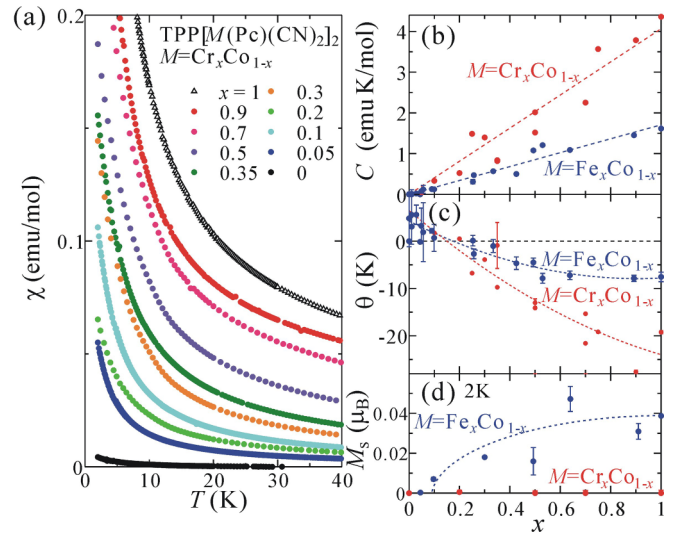


FIG. 3. (a) Magnetic susceptibility in  $M = \text{Cr}_x\text{Co}_{1-x}$  of  $\text{TPP}[\text{M}(\text{Pc})(\text{CN})_2]_2$ . (b) Variation of Curie constant  $C$  with respect to localized spin density  $x$ . (c) Weiss temperature  $\theta$ . (d) Spontaneous magnetization  $M_s$  per transition metal ion measured at 2 K. The red and blue circles correspond to the data in  $M = \text{Cr}_x\text{Co}_{1-x}$  and  $M = \text{Fe}_x\text{Co}_{1-x}$ , respectively. The dashed curves are guides for the eye.

Let us consider the dependence of the magnetic properties on the localized-spin density. Figure 3(a) displays the temperature dependence of the magnetic susceptibility in  $M = \text{Cr}_x\text{Co}_{1-x}$ . The magnetic susceptibility increases with the localized-spin (Cr) density  $x$ . Similar dependence is seen in  $M = \text{Fe}_x\text{Co}_{1-x}$  reported in our previous paper [23]. As shown in Fig. 3(b), the estimated Curie constant  $C$  increases with the ratio  $x$  in  $M = \text{Cr}_x\text{Co}_{1-x}$  and  $M = \text{Fe}_x\text{Co}_{1-x}$  [23], as indicated by red and blue circles, respectively. The Curie constant in  $x=1$  ( $M = \text{Cr}$ ) is close to the value  $C = 3.7$  ( $\text{emu K/mol}$ ) expected in the Heisenberg spin of  $S = 3/2$ . The Weiss temperature  $\theta$  estimated by the magnetic susceptibility is displayed in Fig. 3(c). The negative value of  $\theta$  indicates the averaged antiferromagnetic interaction between the  $d$  localized spins. As  $x$  decreases, the absolute value of  $\theta$  decreases, suggesting that the number of the adjacent  $d$  localized spins decreases.

In  $x=1$  ( $M = \text{Fe}$ ), the  $d$  localized spin exhibits an antiferromagnetic order, with the magnetic easy axis aligned parallel to the CN-ligand direction [27]. As illustrated in Fig. 1(c), the  $\pi$  conduction electron establishes a charge order and becomes spin-polarized due to the ferromagnetic interaction  $J_{\pi d}$ . This polarization aligns the spin of the  $\pi$  conduction electron in parallel with the  $d$  localized spin [12]. As a result, the spin polarization of the  $\pi$  conduction electron in the charge-rich site is more pronounced than that in the charge-poor site. Since the spin-polarization direction in the charge-rich sites is arranged by the  $J_{dd}$  interaction, spontaneous magnetization appears.

We investigated the localized-spin density dependence of the spontaneous magnetization  $M_s$ , as shown in Fig. 3(d). In  $M = \text{Fe}_x\text{Co}_{1-x}$ , the spontaneous magnetization  $M_s$  is observed even in the range down to  $x = 0.1$ . In this low  $x$  range,

since the  $d$  localized spins are no longer adjacent to each other, the  $J_{dd}$  interaction hardly works. Thus, the conventional mechanism for the spontaneous magnetization in  $x = 1$  is not relevant for the low  $x$  range. The origin of the spontaneous magnetization observed in the low  $x$  range is discussed below in Theoretical Analyses.

On the other hand, spontaneous magnetization is not observed in  $M = \text{Cr}$ . Though the  $\pi$  conduction electron is spin polarized by the  $d$  localized spin, these spins are not aligned in a specific direction owing to the Heisenberg-type character of the  $d$  localized spin. Hence, the presence of Ising-spin characteristics in  $d$  localized spin, as observed in  $M = \text{Fe}_x\text{Co}_{1-x}$ , serves as the essential requirement for spontaneous magnetization.

#### IV. THEORETICAL ANALYSES

In this section, we provide theoretical arguments on the electronic states in  $M = \text{Fe}_x\text{Co}_{1-x}$  of  $\text{TPP}[M(\text{Pc})(\text{CN})_2]_2$ . For the  $\pi$  conduction electrons, we use the standard one-dimensional extended Hubbard model at quarter filling,  $N = L/2$  ( $N$ : the number of  $\pi$  conduction electrons,  $L$ : the number of lattice sites) with on-site ( $U$ ) and nearest-neighbor ( $V$ ) interactions. The Hamiltonian for the  $\pi$  conduction electrons is given by

$$H_{\text{EHM}} = -t \sum_{j=1}^L \sum_{\sigma} (c_{j,\sigma}^{\dagger} c_{j+1,\sigma} + \text{H.c.}) + U \sum_{j=1}^L n_{j,\uparrow} n_{j,\downarrow} + V \sum_{j=1}^L n_j n_{j+1}, \quad (2)$$

where  $c_{j,\sigma}$  represents the annihilation operator of the  $\pi$  electron at the  $j$ th site with spin  $\sigma$  ( $=\uparrow, \downarrow$ ). Here  $t$  is the hopping between the nearest-neighbor sites, and  $n_{j,\sigma} = c_{j,\sigma}^{\dagger} c_{j,\sigma}$  and  $n_j = n_{j,\uparrow} + n_{j,\downarrow}$  are the density operators. For the  $d$  localized spins of  $M = \text{Fe}$ , we consider the Ising model with the anti-ferromagnetic exchange interaction  $J_{dd}$ ,

$$H_{\text{Ising}} = J_{dd} \sum_{j=1}^L S_j S_{j+1} r_j r_{j+1}, \quad (3)$$

where  $S_j$  represents the spin variable of the  $d$  localized spins and takes  $S_j = \pm 1/2$ . To describe both the  $M = \text{Fe}$  site ( $S = 1/2$ ) and the  $M = \text{Co}$  site ( $S = 0$ ) in this model, we introduce the parameter  $r_j$ , which takes  $r_j = 1$  for the  $M = \text{Fe}$  site, while  $r_j = 0$  for the  $M = \text{Co}$  site. For the coupling between the  $\pi$  conduction electrons and the  $d$  localized spins, we consider the ferromagnetic Ising-type  $\pi$ - $d$  exchange interaction: its Hamiltonian is given by

$$H_{\pi d} = -J_{\pi d} \sum_{j=1}^L s_j S_j r_j, \quad (4)$$

where  $s_j$  is the spin operator of the  $\pi$  conduction electrons given by  $s_j \equiv (n_{j,\uparrow} - n_{j,\downarrow})/2$ . The parameter  $r_j$  is also introduced to describe both the  $M = \text{Fe}$  and  $\text{Co}$  sites. The full Hamiltonian is given by  $H = H_{\text{EHM}} + H_{\text{Ising}} + H_{\pi d}$ . We imposed the periodic boundary condition.

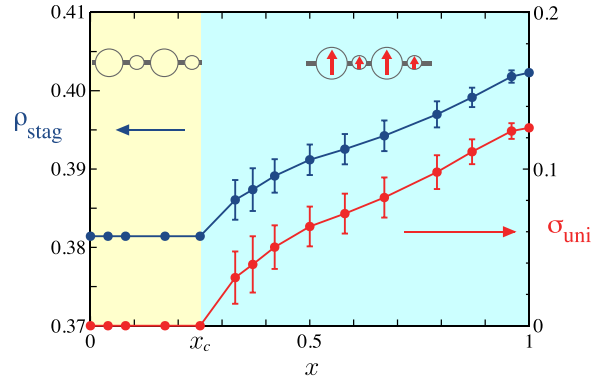


FIG. 4. Order parameter of the charge order  $\rho_{\text{stag}}$  (blue) and the uniform component of the magnetic moment  $\sigma_{\text{uni}}$  (red) as a function of the  $d$  localized spin concentration  $x$  for  $U/t = 4.0$ ,  $V/t = 3.4$ ,  $J_{dd}/t = 0.8$ , and  $J_{\pi d}/t = 2.8$  at  $T/t = 1.0$ . The system size is  $L = 24$ . Here, the error bars express standard deviations of the average over the position of  $d$  localized spins. The schematic illustrations of the charge and spin configurations are indicated, where the sizes of circles and arrows indicate the amounts of charge and spin, respectively.

#### A. Mean-field analysis

First, we apply the mean-field method and analyze the model in real space. We take an average over the position of the localized spins, i.e., the pattern of  $\{r_j\}$  with fixed concentration  $x$ . The  $x$  dependencies of the order parameters for charge order  $\rho_{\text{stag}}$  and spin  $\sigma_{\text{uni}}$  are shown in Fig. 4, where  $U/t = 4.0$ ,  $V/t = 3.4$ ,  $J_{dd}/t = 0.8$ , and  $J_{\pi d}/t = 2.8$  at  $T/t = 1.0$  (see Supplemental Material (SM) for detailed information [28,29]). Here,  $\rho_{\text{stag}} \equiv \langle \sum_j | \langle n_j \rangle_{\text{th}} - \langle n_{j+1} \rangle_{\text{th}} | \rangle_{\text{loc}} / (2L)$  and  $\sigma_{\text{uni}} \equiv \langle \sum_j | \langle s_j \rangle_{\text{th}} | \rangle_{\text{loc}} / L$ , where  $\langle \cdots \rangle_{\text{th}}$  and  $\langle \cdots \rangle_{\text{loc}}$  represent the thermal average and the average over the location of the  $d$  localized spins, respectively. Here  $\sigma_{\text{uni}}$  is the uniform component of the spins of the  $\pi$  conduction electrons. We note that the above definitions of the order parameters are used to avoid unexpected suppression of these quantities due to the domain structure in the presence of  $d$  localized spin inhomogeneity. The error bars for each data set express standard deviations based on the average with respect to localized spins. As seen in Fig. 4, a critical value of the spin concentration  $x_c$  ( $\approx 0.25$ ) is evident. For  $0 < x < x_c$  (yellow region), the order parameter of the charge order stays constant and the uniform component of the magnetic moment is absent. Note that the standard deviations of both quantities are also zero. On the other hand, for  $x_c < x < 1$  (light-blue region),  $\rho_{\text{stag}}$  is enhanced while  $\sigma_{\text{uni}}$  becomes nonzero and increases as a function of  $x$ . These results give us the following picture. When the  $d$  localized spins are too dilute to interact with each other, the  $\pi$  conduction electrons are insensitive to the presence of the  $d$  localized spins. On the other hand, when  $x$  exceeds the critical value  $x_c$ , the  $d$  localized spins can effectively interact with one another, influencing the  $\pi$  conduction electrons and resulting in an amplification of mutual interactions among  $\pi$  electrons. It should be noted that the fluctuations of both quantities among samples become larger for  $x \gtrsim x_c$ .

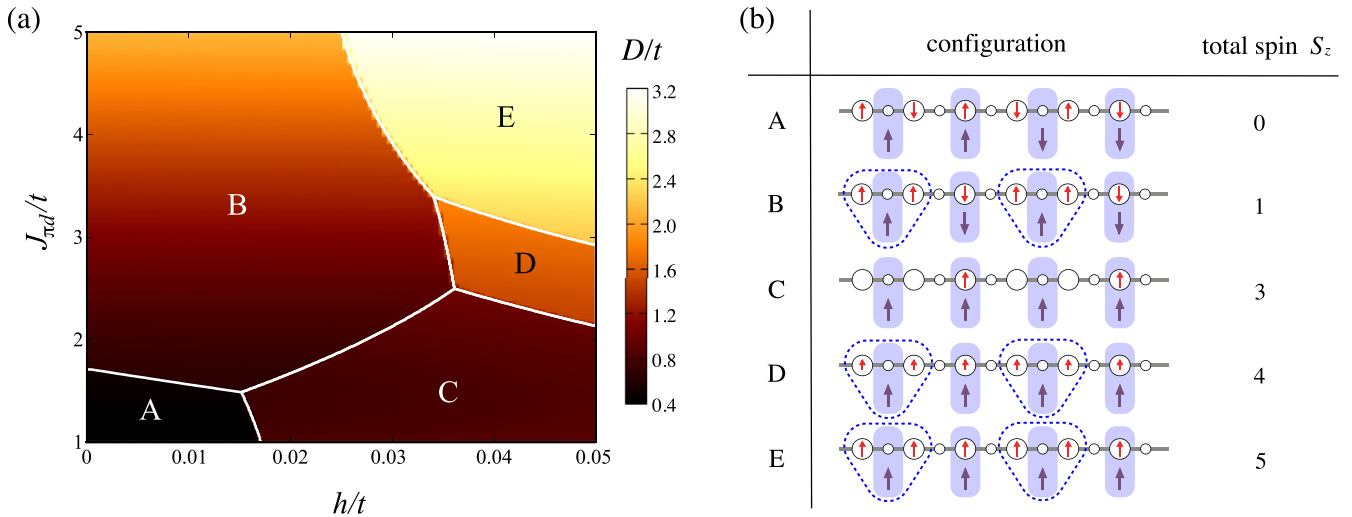


FIG. 5. (a) Ground-state phase diagram of the 12-site cluster system, obtained by the Lanczos exact-diagonalization method. The parameters are set as  $U/t = 6$  and  $V/t = 2.5$ . The coherent component of the optical conductivity  $D$  is also indicated as a contour plot. (b) Configurations and the total spin in respective phases. The purple arrows indicate the  $d$  localized spins and the red arrows indicate the  $\pi$  conduction spins. The sizes of circles indicate the amounts of the charges. The dotted circles indicate the ferromagnetic cluster induced by the localized-spin-assisted ferromagnetic superexchange interaction (see text).

### B. Exact-diagonalization analysis

From the mean-field analysis, we observed spontaneous magnetization at  $x > x_c$ . Especially in the critical region  $x \approx x_c$ , the direct interaction between the  $d$  localized spins is essentially killed and the fluctuations among the samples are substantially enhanced (Fig. 4). In this scenario, the domain structure is not simple. To clarify the mechanism underlying spontaneous magnetization, we next analyzed the ground-state properties by utilizing the exact-diagonalization method.

We employed the Lanczos method [30] for a small cluster with the system size  $L = 12$ . We introduced four  $d$  localized spins, corresponding to the concentration  $x = 0.33$ . For brevity, we restricted ourselves to where the  $d$  localized spins are located at sites with threefold periodicity, as shown in Fig. 5(b). Even in this simplified situation, we found that several states compete and degenerate in the low-energy regions and that the ground states change drastically by the magnetic field. Since the  $d$  localized spins are treated as classical ones, the ground state is determined by comparing the energies for all possible spin configurations.

Figure 5(a) shows the ground-state phase diagram on the plane of the magnetic field  $h$  and the exchange coupling  $J_{\pi d}$ . Here, we introduce the effect of the Zeeman coupling, given by

$$H_h = -h \sum_{j=1}^L (s_j + S_j r_j). \quad (5)$$

The charge and spin configurations of the  $\pi$  conduction electrons and the  $d$  localized spins in the respective states are schematically shown in Fig. 5(b). These configurations were determined through spin/charge structure factor analysis (see SM for detailed information [28]). We found that the charge ordering with twofold periodicity appears in all phases due to the intersite Coulomb repulsion  $V$ . However,

the spin configurations change in respective phases. In state A, the  $\pi$  conduction electrons exhibit an antiferromagnetic pattern on the charge-rich sites due to the antiferromagnetic superexchange interaction within the  $\pi$ -electron orbitals. In state B, the spin configurations change, owing to the strong exchange  $J_{\pi d}$ . The  $d$  localized spins in the charge-poor sites change the direction of the spins of the  $\pi$  conduction electrons in the neighboring charge-rich sites [indicated by the dotted circles in Fig. 5(b)]. As a result, the  $\pi$  conduction electrons in proximity to the  $d$  localized spin sites have ferromagnetic interaction, and two  $\pi$  conduction electrons and a  $d$  localized spin form an effective  $S = 3/2$  spin cluster. This ferromagnetic interaction among the  $\pi$  conduction electrons is induced by the higher-order hopping processes, in which the  $\pi$  conduction electrons hop to the neighboring  $d$  localized spin site and interact with the  $d$  localized spins at the intermediate state. Incidentally, the neighboring  $S = 3/2$  spin (in dotted circles) and  $S = 1$  spin (at the charge-rich site) have antiferromagnetic interactions. Consequently, the ferrimagnetic configuration is realized. This *localized-spin-assisted ferromagnetic superexchange mechanism* is distinctive to systems with diluted  $d$  localized spins. The appearance of spontaneous magnetization can be attributed to this mechanism.

We also found that the ground-state phases are sensitive to the weak magnetic field. In state C, the  $d$  localized spins align ferromagnetically. In state D, the above-mentioned localized-spin-assisted superexchange mechanism works owing to strong  $J_{\pi d}$ , and the net ferromagnetic configurations are realized. State E is the perfect ferromagnetic state.

We also analyzed the transport properties in the respective phases. The optical conductivity  $\sigma(\omega)$  can be analyzed for small cluster-size systems. By combining the sum rule, we evaluate the coherent (or Drude) part  $D$  (see SM for detailed formalism) [28,30,31]. The contour plot of  $D$  is also indicated in Fig. 5 (a). Despite the minimal  $h$  dependence of  $D$  observed in pure electron systems (where  $J_{\pi d} = 0$ ), we identified a

substantial  $h$  dependence in the  $\pi$ - $d$  system. For instance, with  $J_{\pi d}/t = 3$ , we found  $D/t \approx 1.2$  ( $0 < h/t < 0.035$ ),  $D/t \approx 1.7$  ( $0.036 < h/t < 0.046$ ), and  $D/t \approx 2.2$  ( $0.046 < h/t < 0.05$ ). This underscores that the coherent portion of the optical conductivity  $D$  is bolstered by the presence of a weak magnetic field.

## V. SUMMARY AND DISCUSSION

As discussed in Fig. 2(b), in the absence of the localized spin ( $x = 0$ ), the  $\alpha$  value, the exponent in the VRH, is  $\approx 0.7$ . In low localized-spin density ( $x \lesssim 0.1$ ), the  $\alpha$  value decreases with the increase of the localized-spin density  $x$  in  $M = \text{Cr}_x\text{Co}_{1-x}$  and  $M = \text{Fe}_x\text{Co}_{1-x}$ , suggesting the increase of the disorder. The introduced  $d$  localized spins exhibit characteristics akin to magnetic impurities, contributing to the creation of a magnetic random potential. As shown in Figs. 1(d)–1(f), negative magnetoresistance is observed in  $x \gtrsim 0.05$ . This is because the magnetic field aligns the localized spins and reduces the randomness of the magnetic potential.

In the intermediate localized-spin density ( $x \gtrsim 0.1$ ), the  $\alpha$  value rises with  $x$  [Fig. 2(b)]. The introduced localized spins no longer increase the randomness of the magnetic potential for the  $\pi$  conduction electron. As discussed in Fig. 4, the localized spins enhance the charge-order component  $\rho_{\text{stag}}$  of the  $\pi$  conduction electron above the critical density  $x_c$ . Indeed, the experimentally obtained  $T_0^\alpha$  value [Fig. 2(c)] increases clearly with  $x$  in  $x \gtrsim 0.2$ . Here, note that  $T_0^\alpha$  corresponds to the activation energy  $\Delta$  in  $\alpha \rightarrow 1$ . The spontaneous magnetization  $M_s$  [Fig. 3(d)] was observed in  $x \gtrsim 0.1$ . This is again in agreement with the uniform spin component  $\sigma_{\text{uni}}$  above the critical density  $x_c$  (Fig. 4). In this intermediate density, though the  $d$  localized spins are not adjacent to each other, as discussed in state B of Fig. 5(b), the *localized-spin-assisted*

*ferromagnetic superexchange interaction* causes the ferrimagnetic state.

Finally, we discuss the origin of the enhancement of the giant magnetoresistance observed in  $x \approx 0.3$ . As discussed in Fig. 4, the error bars of  $\sigma_{\text{uni}}$  are large just above the critical density  $x_c$ . This indicates that the spin fluctuation is rather large and that a lot of degenerate states exist. Indeed, as shown in Fig. 5, many states, whose energy difference is quite small, compete with each other and coexist locally within the sample. The weak magnetic field can induce changes in these local states, in the way such as the transition from states B into states C, D, or E. The coherent part of the optical conductivity including the direct-current component is enhanced in the transition from states B into states C, D, or E. The calculations are performed within a finite size, and the coherent part of the conductivity changes discontinuously. As the system size increases, many intermediate states are expected, and thus the conductivity is anticipated to change smoothly as a function of the magnetic field. Our theoretical results are consistent with the observed giant negative magnetoresistance.

## ACKNOWLEDGMENTS

The authors would like to thank A. Kayano, H. Tajima, and T. Inabe for valuable discussions. This work was financially supported by the Grant-in-Aid for Scientific Research (JSPS Grants No. 20H05621, No. 23K03322, No. 23K04525, and No. 21H00147) in MEXT, Japan. This work was carried out, in part, at the Center for Spintronics Research Network (CSRN), Graduate School of Engineering Science, Osaka University.

N.H., M.T., and H.Y. contributed equally to this paper. All the authors discussed the results and commented on the paper.

- 
- [1] M. N. Baibich, J. M. Broto, A. Fert, F. Nguyen Van Dau, F. Petroff, P. Etienne, G. Creuzet, A. Friederich, and J. Chazelas, *Phys. Rev. Lett.* **61**, 2472 (1988).
- [2] Y. Tokura and N. Nagaosa, *Science* **288**, 462 (2000).
- [3] H. Kuwahara, Y. Tomioka, A. Asamitsu, Y. Moritomo, and Y. Tokura, *Science* **270**, 961 (1995).
- [4] E. Ribera, C. Rovira, J. Veciana, J. Tarrés, E. Canadell, R. Rousseau, E. Molins, M. Mas, J.-P. Schoeffel, J.-P. Pouget, J. Morgado, R. T. Henriques, and M. Almeida, *Chem. Eur. J.* **5**, 2025 (1999).
- [5] E. Coronado, J. R. Galán-Mascarós, Carlos J. Gómez-García, and V. Laukhin, *Nature (London)* **408**, 447 (2000).
- [6] S. Uji, H. Shinagawa, T. Terashima, T. Yakabe, Y. Terai, M. Tokumoto, A. Kobayashi, H. Tanaka, and H. Kobayashi, *Nature (London)* **410**, 908 (2001).
- [7] E. Coronado and P. Day, *Chem. Rev.* **104**, 5419 (2004).
- [8] T. Komeda, H. Isshiki, J. Liu, Y.-F. Zhang, N. Lorente, K. Katoh, B. K. Breedlove, and M. Yamashita, *Nat. Commun.* **2**, 217 (2011).
- [9] E. Coronado, *Nat. Rev. Mater.* **5**, 87 (2020).
- [10] M. Matsuda, T. Naito, T. Inabe, N. Hanasaki, H. Tajima, T. Otsuka, K. Awaga, B. Narymbetov, and H. Kobayashi, *J. Mater. Chem.* **10**, 631 (2000).
- [11] M. Ikeda, T. Kida, T. Tahara, H. Murakawa, M. Nishi, M. Matsuda, M. Hagiwara, T. Inabe, and N. Hanasaki, *J. Phys. Soc. Jpn.* **85**, 064713 (2016).
- [12] H. Murakawa, A. Kanda, M. Ikeda, M. Matsuda, and N. Hanasaki, *Phys. Rev. B* **92**, 054429 (2015).
- [13] R. Sánchez-de-Armas and C. J. Calzado, *J. Phys. Chem. A* **122**, 1678 (2018).
- [14] H. Seo and H. Fukuyama, *J. Phys. Soc. Jpn.* **66**, 1249 (1997).
- [15] H. Seo, J. Merino, H. Yoshioka, and M. Ogata, *J. Phys. Soc. Jpn.* **75**, 051009 (2006).
- [16] H. Yoshioka, *J. Phys. Soc. Jpn.* **75**, 034703 (2006).
- [17] H. Yoshioka, Y. Otsuka, and H. Seo, *Crystals* **2**, 996 (2012).
- [18] N. Hanasaki, K. Masuda, K. Kodama, M. Matsuda, H. Tajima, J. Yamazaki, M. Takigawa, J. Yamaura, E. Ohmichi, T. Osada, T. Naito, and T. Inabe, *J. Phys. Soc. Jpn.* **75**, 104713 (2006).
- [19] Y. Otsuka, H. Seo, and Y. Motome, *Physica B* **405**, S317 (2010).
- [20] C. Hotta, *Phys. Rev. B* **81**, 245104 (2010).
- [21] N. Hanasaki, H. Tajima, M. Matsuda, T. Naito, and T. Inabe, *Phys. Rev. B* **62**, 5839 (2000).

- [22] N. Hanasaki, M. Matsuda, H. Tajima, E. Ohmichi, T. Osada, T. Naito, and T. Inabe, *J. Phys. Soc. Jpn.* **75**, 033703 (2006).
- [23] M. Ikeda, A. Kanda, H. Murakawa, M. Matsuda, T. Inabe, H. Tajima, and N. Hanasaki, *J. Phys. Soc. Jpn.* **85**, 024713 (2016).
- [24] H. Yoshioka, H. Seo, and Y. Otsuka, *J. Korean Phys. Soc.* **63**, 383 (2013).
- [25] Y. Otsuka, H. Seo, and Y. Motome, *J. Phys. Soc. Jpn.* **83**, 083703 (2014).
- [26] R. Ishii, H. Murakawa, M. Nishi, M. Matsuda, H. Sakai, and N. Hanasaki, *J. Cryst. Growth* **487**, 92 (2018).
- [27] H. Tajima, G. Yoshida, M. Matsuda, K. Nara, K. Kajita, Y. Nishio, N. Hanasaki, T. Naito, and T. Inabe, *Phys. Rev. B* **78**, 064424 (2008).
- [28] See Supplemental Material at <http://link.aps.org/supplemental/10.1103/PhysRevB.108.205114> for detailed information of the theoretical calculations.
- [29] A. Kayano and H. Yoshioka (unpublished).
- [30] E. Dagotto, *Rev. Mod. Phys.* **66**, 763 (1994).
- [31] H. Nakano and M. Imada, *J. Phys. Soc. Jpn.* **68**, 1458 (1999).